Translational Oncology
www.transonc.com

Volume 4 Number 6 December 2011 pp. 355–364 355

Near-infrared Optical Imaging of Exposed Phosphatidylserine in a Mouse Glioma Model[1]

Dawen Zhao*, Jason H. Stafford†, Heling Zhou* and Philip E. Thorpe†

*Department of Radiology, UT Southwestern Medical Center, Dallas, TX, USA; †Department of Pharmacology, UT Southwestern Medical Center, Dallas, TX, USA

Abstract

Phosphatidylserine (PS) is normally intracellular but becomes exposed on the luminal surface of vascular endothelial cells in tumors. It also becomes exposed on tumors cells responding to therapy. In the present study, we optically imaged exposed PS *in vivo* using PGN635, a novel monoclonal antibody that binds PS. The F(ab')$_2$ fragment of PGN635 was labeled with the near-infrared (NIR) dye, IRDye800CW. *In vivo* dynamic NIR imaging was performed after injection of 800CW-PGN635 into mice bearing radiation-treated or untreated U87 glioma xenografts growing subcutaneously or orthotopically. NIR optical imaging revealed a clear tumor contrast in nonirradiated subcutaneous U87 gliomas after injection of 800CW-PGN635. The tumor contrast was visible as early as 4 hours later and was maximal 24 hours later (tumor-to-normal tissue ratio [TNR] = 2.8 ± 0.7). Irradiation enhanced the tumor contrast at 24 hours (TNR = 4.0 ± 0.3). Similar results were observed for orthotopic gliomas. Localization of 800CW-PGN635 to tumors was antigen specific because 800CW-Aurexis, a control probe of irrelevant specificity, did not localize to the tumors, and preadministration of unlabeled PGN635 blocked the uptake of 800CW-PGN635. Fluorescence microscopy confirmed that 800CW-PGN635 was binding to PS-positive vascular endothelial cells in nonirradiated gliomas. Irradiation of the gliomas increased PS exposure on both tumor vascular endothelial cells and tumor cells and gave rise to an increase in tumor contrast with 800CW-PGN635 that was predictive of the reduction in tumor growth. 800CW-PGN635 may be a useful new imaging probe for detection of exposed PS in tumors responding to therapy.

Translational Oncology (2011) 4, 355–364

Introduction

Molecular imaging can provide useful information about drug development, patient stratification, and response to therapy [1–3]. Successful cancer imaging requires imaging probes that recognize cancer-specific markers with great specificity and sensitivity. Cell surface–exposed phosphatidylserine (PS) is an attractive target for molecular imaging. PS is strictly located in the inner leaflet of the plasma membrane bilayer in most normal cell types, including the vascular endothelium. Loss of PS asymmetry occurs during apoptosis and necrosis, resulting in the exposure of PS on the external surface of the cells [4]. Much interest has been generated in developing molecular imaging probes that bind to the exposed PS to noninvasively monitor the response of patients' tumors to various treatments from the induction of tumor apoptosis. Annexin V (A5) is the PS-binding ligand that is most widely used for this purpose. Various radiotracers have been conjugated to annexin V for positron emission tomography (PET) or single-photon emission computed tomography (SPECT) imaging in preclinical tumor models and cancer patients [5,6].

It has recently been observed that PS becomes exposed on the outer surface of viable (nonapoptotic) endothelial cells in tumor blood vessels, probably in response to oxidative stresses present in the tumor

Address all correspondence to: Dawen Zhao, MD, PhD, Department of Radiology, UT Southwestern Medical Center, 5323 Harry Hines Blvd, Dallas, TX 75390-9058. E-mail: Dawen.Zhao@UTSouthwestern.edu

[1]This work was supported in part by the National Cancer Institute (1R21 CA141348-01A1), the National Institutes of Health (NIH; Clinical and Translational Science Awards UL1 RR024982) and the Meredith D. Chesler Foundation, Dallas, TX. Imaging was fulfilled by the Southwestern Small Animal Imaging Research Program (U24 CA126608) and the Caliper IVIS Spectrum under the NIH (1S10RR024757-01). The CRi Maestro was provided by the Joint Program in Biomedical Engineering through a Department of Energy grant (DE-FG02-05CH11280). Magnetic resonance imaging experiments were performed in the Advanced Imaging Research Center, an NIH P41-RR02584 facility.

Received 16 May 2011; Revised 5 July 2011; Accepted 6 July 2011

1944-7124/11/ DOI 10.1593/tlo.11178

microenvironment [7,8]. Vascular endothelium in normal tissues does not have exposed PS. Thus, in addition to imaging apoptotic tumor cells, PS-binding probes also image the exposed PS on the tumor vasculature. We have developed a series of monoclonal antibodies that recognize PS with higher specificity than does annexin V [7–10]. The antibodies recognize PS complexed with the PS-binding protein, β_2-glycoprotein 1 (β_2GP1) [10]. The murine antibodies 2aG4 and 3G4 localize to PS-positive blood vessels in multiple tumor models [9,11,12]. The antibodies then induce monocytes to bind to the tumor vasculature and destroy it by antibody-dependent cellular cytotoxicity, leading to tumor growth inhibition [9,12,13]. Antitumor effects of these antibodies are enhanced by chemotherapy [11], radiation [12,13], and hormone-deprivation therapy [14], all of which increase levels of exposed PS in the tumors, and amplify the target for attack by the antibodies. Bavituximab, a chimeric monoclonal PS-targeting antibody, is in advanced clinical trials in patients with lung and breast cancer [15,16].

In the present study, we used a new, fully human PS-targeting antibody, PGN635, which is similar in specificity and affinity to bavituximab ($K_d \approx 10^{-10}$ M). Like bavituximab, PGN635 recognizes exposed PS complexed with the PS-binding plasma protein β_2GP1 [10]. To detect PS, we conjugated the F(ab′)$_2$ fragment of PGN635 with an NIR dye, IRDye800CW, and used optical imaging to study exposed PS on subcutaneous or orthotopic U87 gliomas in athymic mice. Optical imaging is an inexpensive and rapid technique that allows real-time measurements to be made of exposed PS *in vivo*. NIR dyes have advantages over visible fluorophores in that they use excitation and emission wavelengths in the NIR range. NIR light penetrates tissues more deeply than visible light and causes minimal autofluorescence. The NIR dyes therefore allow imaging of deep-seated orthotopic gliomas in the mouse brain [17–19]. To explore whether 800CW-PGN635 could be used to monitor dynamic changes in levels of exposed PS, gliomas were imaged before and after irradiation. Exposed PS was elevated by irradiation, with the maximal tumor-to-normal tissue ratio (TNR) being obtained 24 hours after irradiation. Fluorescence microscopy revealed that irradiation induces PS to become exposed on both the vasculature and the tumor cells themselves. Our findings suggest that 800CW-PGN635 is a useful tool with which to study exposed PS in preclinical animal tumors. These experiments lay the foundation for further development of PGN635 as an imaging agent in clinic.

Materials and Methods

Preparation of PGN635 F(ab′)$_2$ Fragments and Labeling with IRDye800CW

The human monoclonal antibody PGN635 was generated by Affitech A.S. (Oslo, Norway) in collaboration with Peregrine Pharmaceuticals, Inc (Tustin, CA). It was produced under serum-free conditions by Avid Bioservices (Tustin, CA). Aurexis is a human monoclonal antibody that binds to an irrelevant antigen (*Staphylococcus aureus* clumping factor A) and was used as a negative control antibody. PGN635 and Aurexis F(ab′)$_2$ fragments were generated by reacting antibodies with pepsin at a molar ratio of 1:130 (antibody-pepsin) for 1 hour at 37°C. F(ab′)$_2$ fragments (MW = 110 kDa) were purified by FPLC using an S-200 column (Pharmacia, Piscataway, NJ) and PBS running buffer. F(ab′)$_2$ was then reacted with an *N*-hydroxysuccinimide ester derivative of IRDye800CW (Li-COR, Lincoln, NE) at a molar ratio of 1:10 (F[ab′]$_2$-dye) for 2 hours at room temperature. Unreacted dye was separated from the conjugate using a PD-10 desalting column (GE Healthcare, Uppsala, Sweden). Analyses of the final product, based on the absorbance of the dye at 778 nm and the absorbance of the F(ab′)$_2$ at 280 nm, showed that it consisted of approximately two molecules of dye bound to each F(ab′)$_2$ fragment. The products are referred to as 800CW-PGN635 or 800CW-Aurexis throughout the article.

Glioma Models

All animal procedures were approved by the Institutional Animal Care and Use Committee of University of Texas Southwestern Medical Center. Subcutaneous models were established by injecting 2×10^6 human U87MG glioma cells (ATCC, Manassas, VA) in 100 μl of serum-free medium containing 25% Matrigel (BD Biosciences, San Jose, CA) subcutaneously on the right thigh of anesthetized nude mice (n = 4; BALB/c *nu/nu*; Harlan, Indianapolis, IN). For radiation studies, the total of 20 mice included 8 mice implanted with tumor cells on both thighs for imaging study and 12 mice with one thigh tumor for tumor growth study. Orthotopic gliomas were established by making a 1-cm-long incision along the midline of the head of anesthetized nude mice (n = 6) to expose the skull. Using a high-speed drill, a 1-mm burr hole was made in the skull over the right hemisphere, anterior to the coronal fissure. About 10^5 U87 cells in 4 μl of PBS and Matrigel were injected directly into right caudal diencephalon 1.5 mm beneath the dura mater using a 32-gauge Hamilton syringe that causes minimal tissue damage. The burr hole was filled with bone wax, and the scalp was closed with sutures.

Radiation Treatment

When subcutaneous tumors on both thighs reached ~5 mm in diameter, a single dose of 12 Gy of irradiation was delivered to the tumors on the left thigh of anesthetized mice using a small animal irradiator (XRAD320; Precision X-ray, Inc, North Branford, CT) fitted with a variable collimator to generate a single adjustable collimated iso-dose beam of x-rays at a dose rate of 10 Gy/min. In a separate experiment, six animals bearing single subcutaneous tumors (~5 mm in diameter) received a single dose of 12 Gy of radiation to their tumors, whereas another group of six tumor-bearing animals served as controls. Tumor size was measured using calipers twice a week, and tumor volume was calculated using $abc \times 6/\pi$. For the orthotopic gliomas, a single dose of 12 Gy of irradiation was delivered using a D-shaped collimator to the whole brain excluding the olfactory bulb.

Detection and Quantification of Exposed PS In Vivo

Mice bearing two thigh tumors were given a single dose of 12 Gy of irradiation to the left tumor to induce exposed PS. Twenty-four hours later, 150 μg of PGN635 or the control body Aurexis was injected intravenously (i.v.) and allowed to circulate for 4 hours. The mice were anesthetized, exsanguinated, and perfused with heparinized saline. The tumors on both sides and adjacent muscular tissues were removed and frozen for preparation of cryosections. Vascular endothelium was stained using a rat antimouse CD31 antibody (BD Biosciences, San Jose, CA) followed by Cy3-labeled goat anti-rat IgG. PGN635 or Aurexis was detected using biotinylated goat anti-human IgG conjugated to Cy2. Images were captured using a CoolSNAP digital camera (Roper Scientific Photometrics, Tucson, AZ) mounted on Elipse E600 fluorescent microscope (Nikon, Melville, NY) and analyzed with MetaVue software (Universal Imaging Corporation, Downingtown, PA). Doubly labeled endothelial cells (i.e., CD31 positive/

PGN635 positive) were identified by yellow fluorescence on merged images. The percentage of doubly positive vessels was calculated as follows: (mean number of yellow vessels per field / mean number of total vessels) × 100. Ten random 0.079-mm^2 fields were evaluated for each section.

Magnetic Resonance Imaging

Orthotopic gliomas were examined by anatomic magnetic resonance imaging (MRI) using a 9.4-T horizontal bore magnet with a Varian INOVA Unity system (Palo Alto, CA). Each mouse was maintained under general anesthesia (air and 2% isoflurane). T_1- and T_2-weighted fast spin-echo multislice coronal images were acquired. T_1-weighted contrast-enhanced images were acquired after i.v. bolus injection of the contrast agent Gd-DTPA-BMA (0.1 mmol/kg body weight; Omniscan [Amersham Health, Inc, Princeton, NJ]) into a tail vein.

NIR Fluorescence Imaging

When the subcutaneous tumors reached ~5 mm in diameter, *in vivo* fluorescence imaging was performed using a Maestro imaging system (CRi, Inc, Woburn, MA). Each mouse was maintained under general anesthesia (air and 2% isoflurane). NIR images were acquired before and at different times after administration of 800CW-PGN635 or 800CW-Aurexis (2 nmol/mouse) through a tail vein. For the irradiated tumors, the NIR dye–labeled conjugates were injected 24 hours after irradiation, and imaging was carried out periodically for 24 hours. For the antibody competition study, unlabeled PGN635 was injected i.v. at 2.5 mg/kg 4 hours before administration of 800CW-PGN635. A set of filters specifically for NIR imaging (excitation, 671-705 nm; emission, 730-950 nm) was applied. For the orthotopic gliomas, NIR imaging was initiated after MRI confirmed an intracranial tumor with a diameter of ~5 mm. The tumor-bearing mice were anesthetized and imaged for 24 hours. Immediately after the last image at 24 hours, the skull of the mouse was surgically removed to expose both sides of the brain tissues and a last *in vivo* image was obtained. The whole surgical procedure and imaging were completed within 10 minutes under anesthesia, and no obvious bleeding occurred.

Analysis of Fluorescence Imaging

Fluorescence images were processed with the Maestro software 2.8. The spectrum of background signal (peak emission, ~770 nm) was first obtained from a mouse before the 800CW-antibody conjugate injection, whereas the spectrum of 800CW conjugates (peak emission, ~800 nm) was detected from a solution of the dye in PBS. The spectra

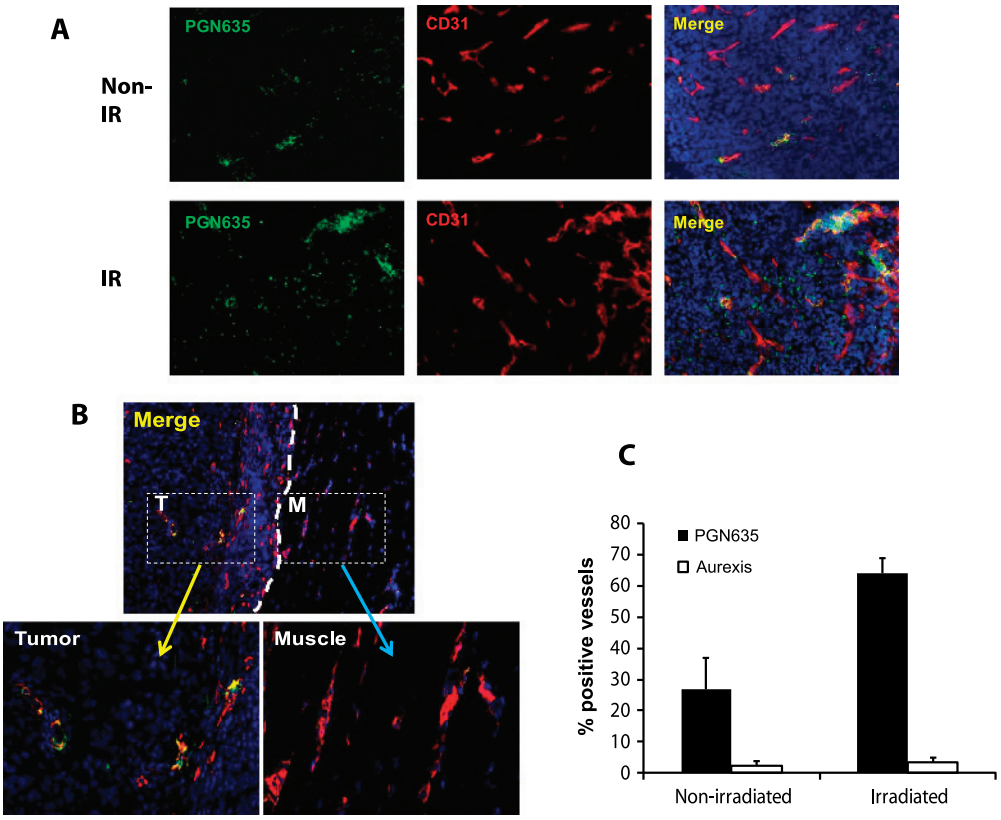

Figure 1. Immunohistochemical study of localization of PGN635 antibody in nonirradiated and irradiated tumors. Mice bearing a subcutaneous U87 glioma on each thigh received a single dose of 12 Gy of irradiation to the left side tumor. Exposure of PS was determined 24 hours later by i.v. injection of full-length PGN635 or control antibody Aurexis. Animals were perfused with saline 3 hours later. (A) Frozen sections of nonirradiated and irradiated tumors were analyzed for the presence of fluorescently labeled PGN635 (green). Vascular endothelial cells were counterstained with anti-CD31 (red). Merged images revealed coincidence of staining showing that PGN635 was bound to vascular endothelial cells in the nonirradiated tumor. Increased PGN635 staining was seen in the irradiated tumors and was due to increased staining of both endothelial cells and tumor cells. Tumor sections from control animals that had been injected with Aurexis were essentially unstained (not shown). (B) The tumor tissues and adjacent muscular tissues, both of which received a single dose of 12 Gy of radiation, were used for PGN635 staining. In contrast to abundant positive staining seen in tumor vessels, the muscle showed essentially no positively stained vessels. (C) Irradiation increased the percentage of PS-positive vessels from 27% ± 10% to 64% ± 6% ($P < .001$). Staining with PGN635 was antigen specific because Aurexis gave low levels of staining.

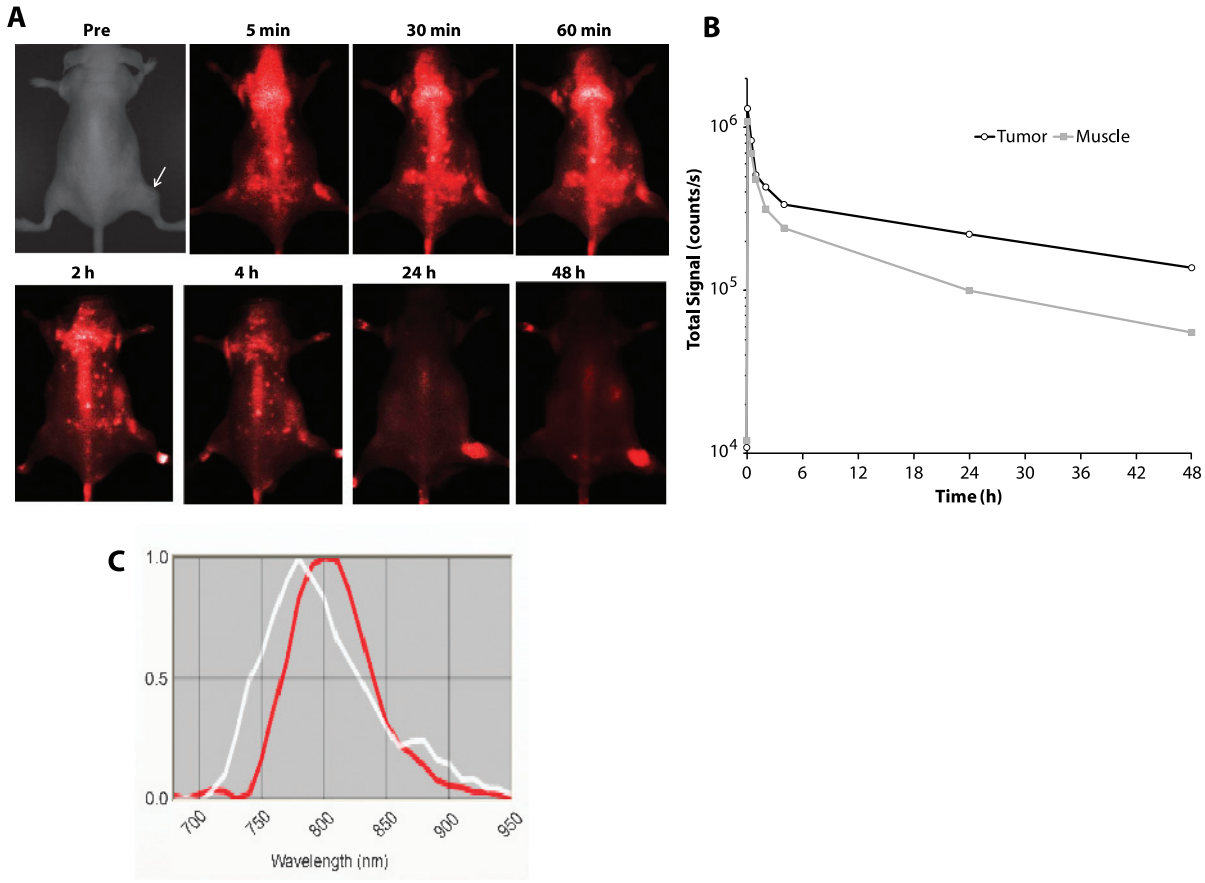

Figure 2. *In vivo* NIR imaging of baseline level of PS in a subcutaneous glioma. (A) A mouse bearing a representative subcutaneous U87 glioma on the right thigh (arrow) was injected i.v. with 800CW-PGN635, and optical imaging was performed at various time points thereafter. During the first 4 hours, the light signal accumulated in the tumor area. However, by 24 hours, the light signal remained only in the tumor and persisted there for at least 48 hours after injection. (B) Mean light intensity curves for the tumor (open circles) and the contralateral muscle (solid squares) revealed that 800CW-PGN635 rapidly gave signals in both the tumor and the normal muscle but that the tumor signal was sustained while the muscle signal had washed out by 24 hours. The tumor-muscle ratios were 2.2 at 24 hours and 2.4 at 48 hours. (C) Normalized emission spectra showing the NIR PGN635 dye with a peak emission wavelength at ~800 nm (red), whereas the background signal wavelength (white) was at ~770 nm.

were then imported and used to unmix the NIR dye signal from the background signal for both *in vivo* and *ex vivo* studies. The whole set of *in vivo* images of each individual mouse, obtained before and at various times after injection of the dye, was examined for quantification. A common region of interest was based on the most obvious signal of the tumor 24 hours after injection and was applied to both the tumor and the normal tissue of each image. Because exposure time of light varied at different time points, longer exposure times were used for the later time points. The total photon counts were normalized by time (counts/sec) in identical regions of interest and compared to each other to detect dynamic changes in signal intensity. These data were used to construct the histograms in the figures.

Ex Vivo *Fluorescence Imaging*

Immediately after the last *in vivo* image, tumor-bearing mice were killed, and tumor tissues and thigh muscles were dissected. *Ex vivo* fluorescence imaging was performed using the Maestro imaging system.

NIR Fluorescence Microscopy

Immediately after *in vivo* imaging, tumor-bearing mice were killed, and tumor tissues were dissected. The cryosections were immunostained with antibodies to the endothelial marker, CD31 (Serotec, Raleigh, NC) followed by Cy3-conjugated secondary antibody (Jackson Immunoresearch Laboratories, West Grove, PA). The NIR fluorescence signal was detected using a Zeiss AxioObserver (Carl Zeiss MicroImaging, Inc, Thornwood, NY) equipped with NIR filters. The NIR signals were recorded and merged with the CD31 image and the 4′, 6-diamidino-2-phenylindole (DAPI)–stained image of the same field.

Statistical Analysis

Statistical significance was assessed using an analysis of variance on the basis of the Fisher protected least significant difference (StatView; SAS Institute, Inc, Cary, NC) or Student's *t* tests.

Results

Exposed PS on Blood Vessels and Tumor Cells in Gliomas

An average of 27% ± 10% of blood vessels in nonirradiated tumors had exposed PS on their endothelium, as judged by coincident staining of vessels by PGN635 and anti-CD31 (Figure 1, *A-C*). Irradiation increased the levels of exposed PS on tumor vessels to 64% ± 6% ($P < .001$; Figure 1). In addition, irradiation induced PS exposure on

the tumor cells themselves (Figure 1*A*). Tumor cells were identified by their expression of human histocompatibility antigens, as detected by staining with W6/32 antibody (not shown). The localization seen with PGN635 to vessels and tumor cells was antigen specific because the negative control 800CW-Aurexis produced relatively little staining (Figure 1*C*). Furthermore, muscular tissues adjacent to the tumor that received the 12-Gy radiation were found to be essentially devoid of PGN635 staining, compared to the abundant PGN635 staining seen in tumor tissues (Figure 1*B*).

In Vivo *Optical Imaging of Exposed PS in Nonirradiated Gliomas*

800CW-PGN635 localized with high selectivity to subcutaneous U87 tumors in mice. Clear contrast between the tumor and contralateral normal tissue was visible 24 hours after injection and improved still further by 48 hours after injection (Figure 2*A*). Time course studies showed that the light intensity in both the tumor and the normal tissue was maximal 5 minutes after injection and then decreased abruptly during the next 4 hours. However, in contrast to the fast washout in normal tissues, the signal in the tumor was maintained over time. The TNR was 2.2 at 24 hours and 2.4 at 48 hours (Figure 2*B*). The 800CW-labeled F(ab′)$_2$ fragment of PGN635 antibody is cleared from the blood with a half-life of 6 hours (J.H.S., unpublished observations). Thus, the images shown in Figure 2 represent tumor-bound label. Normalized emission spectra of 800CW-PGN635 and background are shown in Figure 2*C*.

Dynamics of Exposed PS in Response to Radiation

A single dose of 12 Gy of irradiation was given to the left side tumor of mice carrying tumors on each thigh. 800CW-PGN635 was injected 24 hours later. As expected, the nonirradiated tumors on the right side gave similar results to those of mice with single tumors (Figure 2) with a maximum TNR of 2.5 ± 0.5 being obtained 24 hours after injection ($P < .05$; Figure 3, *B* and *C*). Irradiation significantly enhanced tumor contrast. A TNR of 2.8 ± 1.1 was obtained 4 hours after injection, rising to 4.0 ± 0.2 24 hours after injection. The ratio of the TNR in the irradiated tumors to that in the nonirradiated tumors was 1.6 at 24 hours after injection. For tumor growth study, the tumors

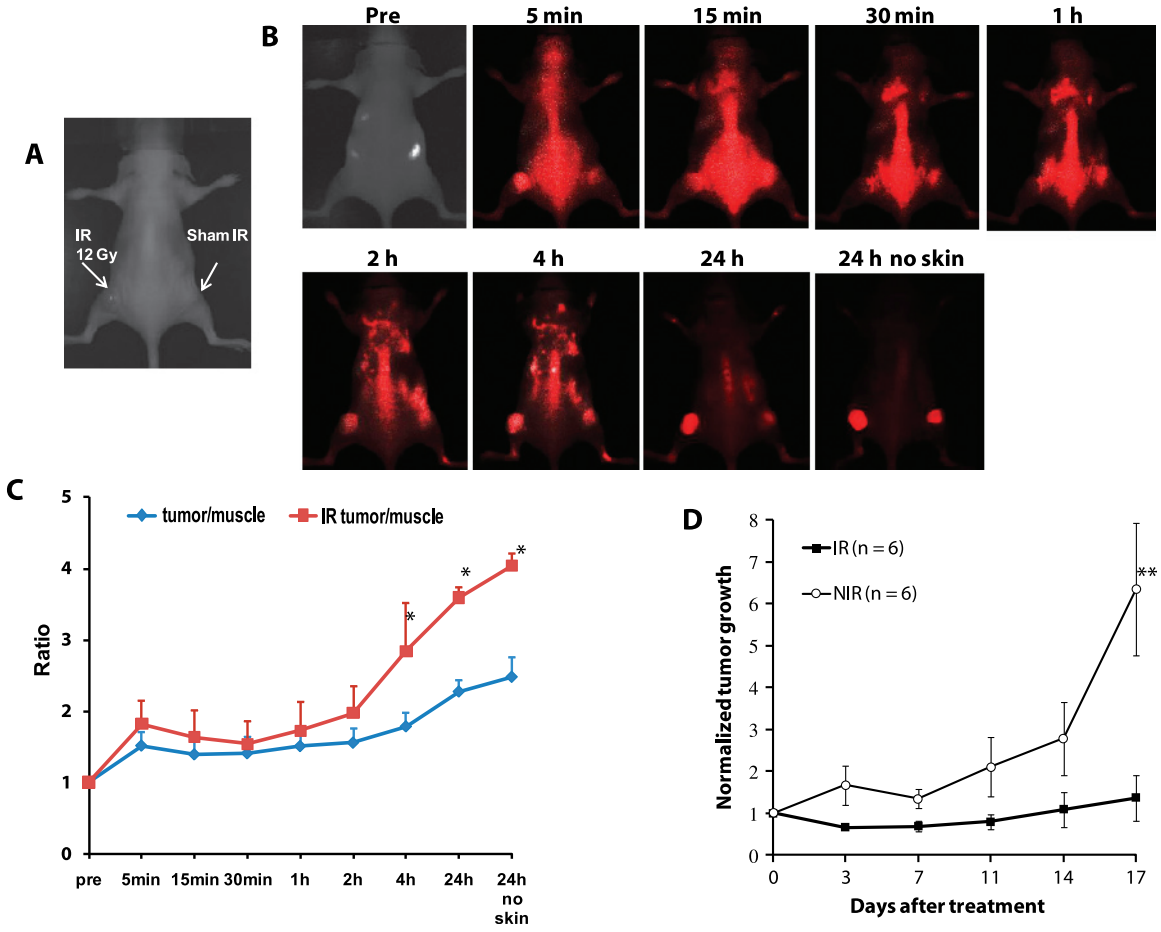

Figure 3. *In vivo* NIR imaging of exposed PS in gliomas before and after irradiation. (A) A mouse bearing representative size-matched subcutaneous U87 tumors on each thigh received 12 Gy of irradiation to the left side tumor. (B) At 24 hours after radiation, 800CW-PGN635 was injected through a tail vein, and a series of *in vivo* fluorescence images was acquired at different time points. The contrast between the nonirradiated tumor on the right side and normal muscle increased during the 24-hour period after injection to a TNR of 2.6. Irradiation of the tumor on the left side increased levels of exposed PS to a TNR of 4.2. *$P < .05$ from non-IR. (C) A time course study revealed that the maximal TNR of 2.5 was achieved at 24 hours for nonirradiated tumors ($n = 4$; blue line). Irradiation increased the TNR of the irradiated tumor to 4.0 at 24 hours ($n = 4$; red line; $P < .05$). (D) Tumor growth curves showed that a single dose of 12 Gy of radiation significantly inhibited tumor growth ($n = 6$), compared with the sham irradiated control tumors ($n = 6$; **$P < .01$).

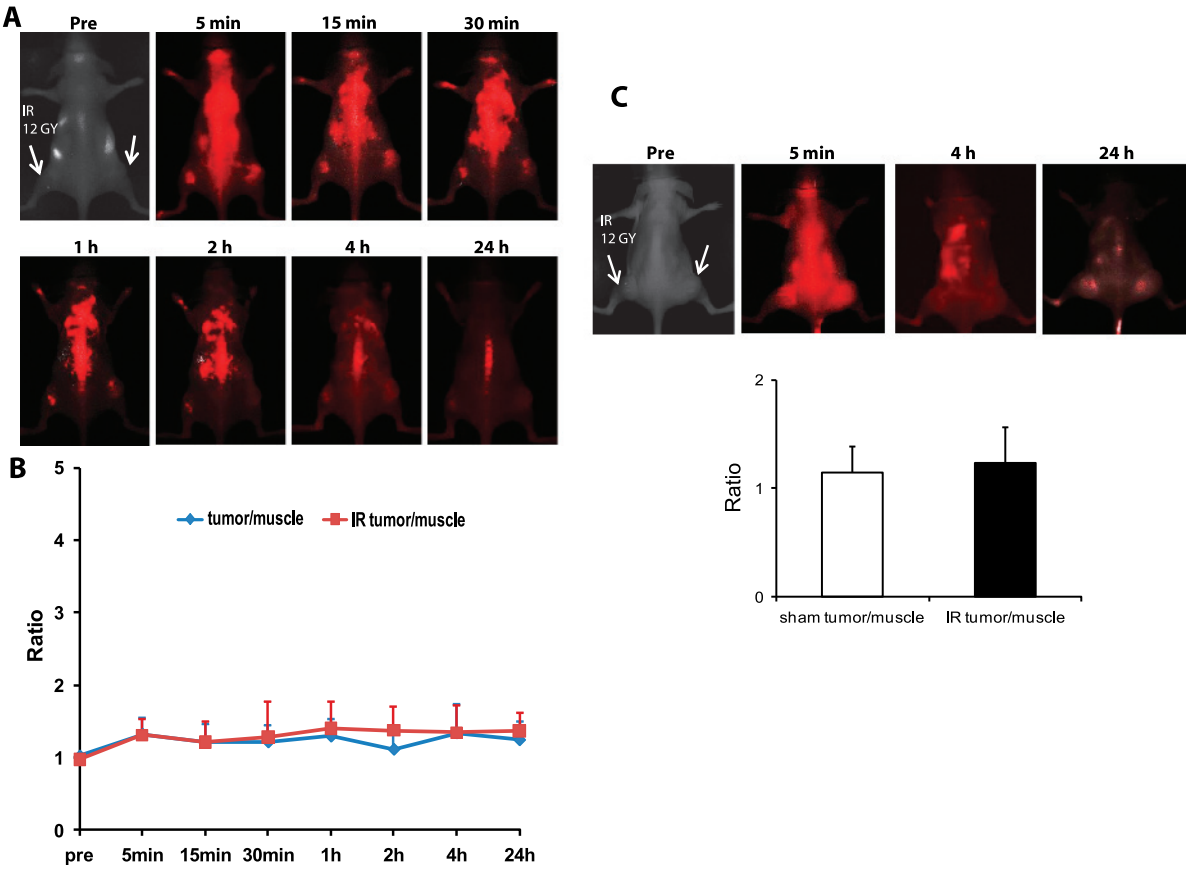

Figure 4. Specificity of 800CW-PGN635 optical probe *in vivo*. (A) To establish the antigen specificity of the 800CW-PGN635 probe, a control probe 800CW-Aurexis was injected into the mice 24 hours after irradiating one of the tumors in the flanks. A series of whole body images was acquired. The 800CW-Aurexis accumulated in both tumors during the first hour. However, both signals diminished thereafter. No signal remained in either tumor 24 hours after injection. (B) A time course study showed that 800CW-Aurexis did not accumulate in either the nonirradiated tumors ($n = 2$) or the irradiated tumors ($n = 2$). (C) A competition study showed that injection of unlabeled PGN635 (2.5 mg/kg, i.v.) 4 hours before imaging blocked 800CW-PGN635 accumulation in both the irradiated tumor (left) and the nonirradiated tumor (right).

($n = 6$) received a single dose of 12 Gy of radiation showed significantly inhibited tumor growth compared with the sham control group ($n = 6$; $P < .01$; Figure 3*D*).

Specificity of 800CW-PGN635

The binding specificity of 800CW-PGN635 was confirmed by comparing its localization pattern with that of the negative control 800CW-Aurexis. Figure 4*A* shows that 800CW-Aurexis entered both the irradiated and the nonirradiated tumors within 30 minutes of injection, but rapidly washed out. No significant contrast remained between either the irradiated or the nonirradiated tumors and normal tissues by 24 hours (Figure 4*B*). Furthermore, preadministration of unlabeled PGN635 before giving the 800CW-PGN635 almost completely blocked localization of the 800CW-PGN635 to both irradiated tumors and nonirradiated tumors (Figure 4*C*).

In Vivo *Optical Imaging of Exposed PS in Orthotopic Gliomas*

800CW-PGN635 successfully imaged U87 gliomas growing in the brains of mice, despite the light having to pass through the skull. Before optical imaging, MRI revealed that the mice had intracranial tumors with a high signal intensity on T_2-weighted images and a ring-shaped contrast enhancement on T_1-weighted contrast enhanced images (Figure 5*A*). A clear light signal that corresponded to the magnetic resonance image of the tumor in location and size was obtained 24 hours after injection of 800CW-PGN635 (Figure 5*B*). The mean tumor signal was 1.3 ± 0.4 for the nonirradiated tumors and 1.6 ± 0.3 for the 12-Gy irradiated tumors. To confirm that the signal originated from the brain tumor, a surgical procedure was performed on anesthetized mice to reflect the scalp and remove the skull to expose the brain. A brighter and more focused light signal was emitted from the region of tumor growth (Figure 5*B*). The TNR for irradiated tumors was significantly higher (4.2 ± 0.4) compared with that (2.1 ± 0.4) for nonirradiated brain tumors ($P < .01$; Figure 5*C*). The improvement in TNR and the difference between nonirradiated and irradiated tumors seen when the skull was removed are probably because both the excitation light and the emitted light are significantly absorbed during passage through the skull and scalp.

NIR Fluorescence Microscopy to Detect 800CW-PGN635 in Tumors

A fluorescence microscope equipped with NIR filters was used to detect 800CW-PGN635 in cryosections (7 μm) prepared from subcutaneous tumors 24 hours after injection of 800CW-PGN635. In good agreement with histologic findings with unconjugated PGN635

(Figure 1), merged images showed that the 800CW-PGN635 was essentially binding exclusively to vascular endothelial cells in nonirradiated tumors (Figure 6). Irradiation increased the percentage of PS-positive vessels and also induced exposed PS on the tumor cells themselves. Thus, the 800CW-PGN635 signal in nonirradiated tumors derives from PS-positive vasculature, whereas the stronger signal in irradiated tumors derives from both PS-positive vasculature and tumor cells.

Discussion

We have demonstrated the feasibility of using PGN635 $F(ab')_2$ labeled with the NIR dye, 800CW, for optical imaging of exposed PS in both subcutaneous and orthotopic mouse models of U87 glioma. Histologic studies showed that the PS signals detected in nonirradiated gliomas by *in vivo* NIR imaging were due to exposed PS on tumor vascular endothelial cells. This is in good agreement with previous studies performed in various tumor models: prostate R3327-AT1 tumors [30], breast cancer MDA-MB231, 4T1 cells [31], lung cancer H460 and A549, and F98 gliomas [12,13]. Irradiation-induced increase in exposed PS was successfully visualized by 800CW-PGN635 optical imaging in mice. Fluorescence microscopy confirmed that both PGN635 and 800CW-PGN635 localized more strongly to the irradiated tumors. In irradiated tumors, both the vessels and the tumor cells were PS positive. The antigen-binding specificity of PGN635 was verified by competition experiments with unconjugated PGN635 and by the lack of staining with the irrelevant control 800CW-Aurexis.

Noninvasive molecular imaging of apoptosis is of clinical importance because it could give an early indication of the responsiveness of a patient's tumor to therapy, allowing alterations in the therapy to be made if the responses were not as good as expected [5,6,20]. In the past several years, much effort has been made in developing molecular imaging agents to monitor tumor responses. Radiolabeled and fluorescent annexin V preparations have been extensively tested in animal studies [21–23]. More recently, clinical studies of PET or SPECT imaging with radiolabeled annexin V have shown that a higher uptake of annexin V by tumors during or after treatment correlates positively with a better prognosis in patients with breast, head and neck, or lung cancer [24–26]. However, not all PS-expressing tumor cells in responding tumors are apoptotic. Hammill et al. [27] found that many of the cells that stain positively for annexin V are viable and can resume growth and reestablish phospholipid asymmetry once the therapy is discontinued. Their results indicate that exposed PS, and thus loss of membrane asymmetry, precedes commitment to apoptotic death.

PGN635, bavituximab, and related murine monoclonal antibodies recognize PS and other anionic phospholipids in a β_2GP1-dependent fashion. The antibodies have a more restricted specificity for PS than does annexin V, which recognizes PE in addition to PS and other anionic phospholipids [7,28,29]. We previously radiolabeled bavituximab with ^{74}As, which is a long-lived positron emitter having a radioactive half-life of 17.8 days, and used it to image the vasculature of Dunning prostate R3227-AT1 tumors in rats. The long half-life of ^{74}As allowed the intact

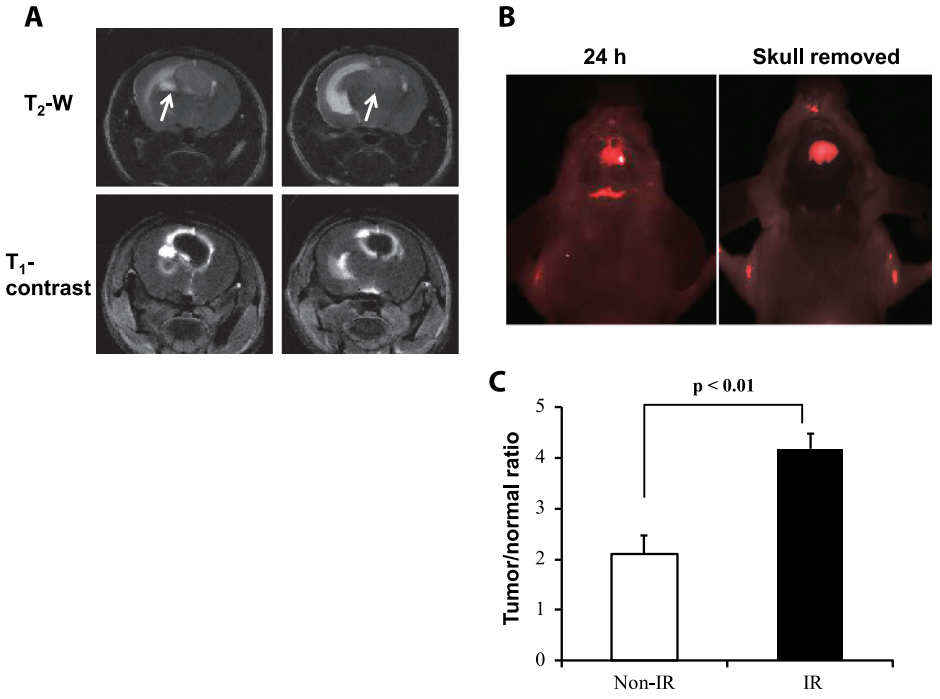

Figure 5. *In vivo* optical imaging of exposed PS in orthotopic gliomas. A mouse bearing a representative orthotopic U87 glioma was irradiated with a single dose of 12 Gy to the whole brain using a D-shaped collimator. (A) Anatomic MRI revealed a 5-mm-diameter intracranial lesion crossing the midline to invade the left side brain on the consecutive T_2-weighted slices. T_1-weighted contrast-enhanced MRI showed the typical ring-shaped enhancement in the tumor periphery. (B) 800CW-PGN635 was injected into the mouse 24 hours after radiation, and dynamic NIR optical imaging was performed. As with the subcutaneous tumors, maximal tumor contrast was achieved 24 hours after injection. Removal of the skull increased the signal, and subsequent dissection confirmed that the signal was from the tumor. (C) The tumor-*versus*-contralateral normal brain ratio TNR was 4.2 ± 0.4 for irradiated tumors (n = 3), which was significantly higher than the TNR of 2.1 ± 0.4 for nonirradiated tumors (n = 3; $P < .01$).

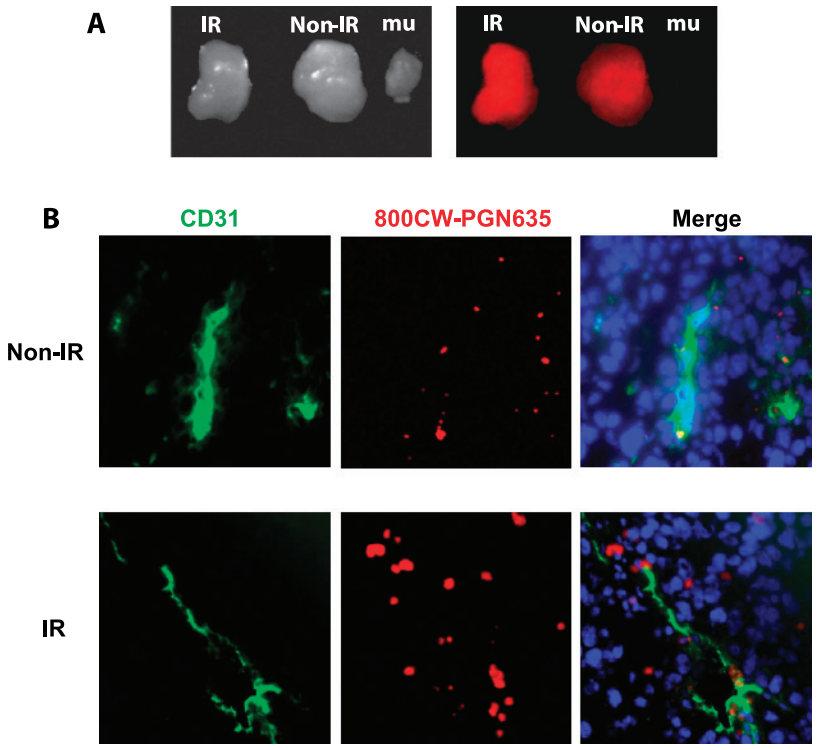

Figure 6. NIR fluorescence microscopy to detect the location of the 800CW-PGN635 optical probe in nonirradiated or irradiated gliomas. (A) Mice bearing subcutaneous gliomas that had been irradiated (IR) or sham-irradiated (non-IR) were injected with 800CW-PGN635 24 hours later. Irradiation increased the tumor signal. The gliomas and contralateral muscle (mu) were excised. (B) Sections of nonirradiated (top row) or irradiated U87 gliomas (bottom row) were examined for the presence of 800CW-PGN635 (red), CD31 (green) or DAPI (blue). Vascular endothelial cells were detected by immunofluorescence staining with anti-CD31 (green). Nuclei were detected with DAPI (blue). NIR signals were detected with an infrared filter. The merged image shows that the PGN635 optical probe colocalized with tumor vascular endothelial cells in the nonirradiated tumor. In contrast, irradiation increased the NIR signal on both the vascular endothelial cells and the tumor cells.

antibody to reach its optimal target to background selectivity at 72 hours without appreciable radioactive decay [30]. Tumor-selective targeting was observed by PET imaging. A maximum tumor-to-liver ratio of 22 was achieved.

In the present study, we used the $F(ab')_2$ fragment of PGN635 for optical imaging to ensure its rapid clearance from the bloodstream and the achievement of high tumor to background ratios by 24 hours after injection. Because the target on vascular endothelial cells is directly accessible to the blood, PGN635 localizes rapidly to tumor vessels. We have previously demonstrated that exposed PS on tumor vessels in orthotopic gliomas is freely accessible to PS-targeting antibodies [12]. Even tumor cells having exposed PS were labeled, probably because local disruption of blood brain barrier occurs in brain tumors. PGN635 is not internalized to any significant extent by cells and so remains for 2 to 3 days on the endothelial cell surface, giving plenty of time for the unbound PGN635 $F(ab')_2$ in the blood to be cleared. We found in the present study that PGN635 labels about 27% of the vessels in nonirradiated U87 gliomas. Different tumors vary in the percentage of their vessels that have exposed PS [7,8,12,13,30]. In Dunning R3227-AT1 prostate tumors, 40% of vessels have exposed PS [30]. In F98 gliomas, the percentage is only 11% [12]. Exposed PS on viable endothelial cells is induced by hypoxia, acidity, and other stresses known to be present in the tumor microenvironment [7]. Differences in PS positivity in different tumors probably relate to the levels of oxidative stresses in the tumor microenvironment [31].

Irradiation of U87 tumors with 12 Gy increased the percentage of tumor vessels that had exposed PS from 27% to 64% and increased the TNR from 2.8 to 4.0. These findings accord with our earlier finding that irradiation of A549 NSCLC xenografts and F98 gliomas increase vascular expression of PS [12,13]. We have previously applied fractionated radiation (2 Gy × 5) to treat H460 lung tumor xenografts. Similar to our current study, the fractionated radiation sufficiently induced PS exposure [13]. Endothelial cells in tumors are highly sensitive to irradiation and expose PS after as little as 5 Gy. Our previous studies have shown that endothelial cells in tumors irradiated with 5 Gy seem to remain viable. They remain morphologically intact and lack markers of apoptosis for several days [13]. In the present study, 12 Gy of irradiation also increased PS exposure on the tumor cells in U87 tumors, thus contributing to the increased localization of 800CW-PGN635 in irradiated tumors. Further studies are needed to determine whether the PS-expressing tumor cells are apoptotic or not.

Optical imaging is increasingly being used in preclinical cancer research [32,33]. It is being used in particular to study cancer-specific markers and drug pharmacokinetics and to monitor drugs' effects in small animals [17,34,35]. The attraction of the technique is that it is inexpensive, is simple to conduct, gives real-time results, and does not require the handling and disposal of radioactive isotopes. In the clinic, optical imaging by visualizing fluorescently labeled tumor cells has recently emerged as an attractive approach to facilitate identification of tumor margins or sentinel lymph node metastases [36,37]. Several

previous studies have demonstrated *in vivo* optical imaging of apoptosis with annexin V labeled with Cy5.5, a red excitable dye [22]. However, the NIR dye IRDye800CW seems to be superior to Cy5.5 for *in vivo* imaging [34]. NIR fluorescence penetrates more deeply into tissues because it has lower tissue absorption and scattering of light and causes relatively little autofluorescence. Our previous study showed that it is possible to image deep-seated orthotopic gliomas in mice with IRDye800-labeled 2-deoxyglucose [18]. Here, we have demonstrated the ability of NIR optical imaging to detect PS translocation in both subcutaneous and orthotopic glioma models.

Clinical applications of optical imaging are currently limited to the detection of tumor margins or deposits during surgery, to the detection of superficial tumors, and to the detection of deep-seated tumors by endoscopy. The current study is also a proof-of-principle study, indicating the potential of this unique antibody for detecting deep-seated tumors using PET, SPECT, or MRI. Other labels besides optical dyes should be considered for attachment to PGN635 $F(ab')_2$ fragments. PGN635 is particularly impressive as a targeting ligand because of its high specificity, lack of uptake by the liver or any other organs, rapid acquisition by its vascular target, and its persistence on the vascular target for days. It is an excellent candidate, for example, for labeling with DOTA and ^{64}Cu for PET or ^{111}In for SPECT. It should have applications not only in tumor imaging but also in the imaging of thrombi or sites of ischemia for cardiovascular investigations. It will also be interesting to correlate PGN635 optical imaging data with functional MRI studies of apoptosis by diffusion-weighted MRI and vascular perfusion or permeability by dynamic susceptibility contrast MRI.

In summary, we have combined NIR optical imaging with PGN635, a novel monoclonal antibody that binds to PS, to monitor *in vivo* dynamics of exposed PS on mouse gliomas. We show that irradiation increases the PS signal, predictive of the response to therapy. The high tumor specificity of PGN635 in the present study underscores the prospects of using PGN635 and related antibodies to treat cancer in humans.

Acknowledgments

The authors thank Peregrine Pharmaceuticals, Inc, Tustin, CA, for the provision of PGN635 antibody. The authors also thank Kwang Song, Timothy Solberg, Debabrata Saha, and Abhijit Bugde for technical support and Ralph Mason for collegial support.

References

[1] Weissleder R and Pittet MJ (2008). Imaging in the era of molecular oncology. *Nature* **452**, 580–589.

[2] Blasberg RG (2007). Imaging update: new windows, new views. *Clin Cancer Res* **13**, 3444–3448.

[3] Schellingerhout D and Gelovani J (2006). Clinical trials in a molecular world. *Neuroimaging Clin N Am* **16**, 681–694, ix.

[4] Balasubramanian K and Schroit AJ (2003). Aminophospholipid asymmetry: a matter of life and death. *Annu Rev Physiol* **65**, 701–734.

[5] Tait JF (2008). Imaging of apoptosis. *J Nucl Med* **49**, 1573–1576.

[6] Blankenberg FG (2008). *In vivo* detection of apoptosis. *J Nucl Med* **49**(suppl 2), 81S–95S.

[7] Ran S, Downes A, and Thorpe PE (2002). Increased exposure of anionic phospholipids on the surface of tumor blood vessels. *Cancer Res* **62**, 6132–6140.

[8] Ran S and Thorpe PE (2002). Phosphatidylserine is a marker of tumor vasculature and a potential target for cancer imaging and therapy. *Int J Radiat Oncol Biol Phys* **54**, 1479–1484.

[9] Ran S, He J, Huang X, Soares M, Scothorn D, and Thorpe PE (2005). Antitumor effects of a monoclonal antibody that binds anionic phospholipids on the surface of tumor blood vessels in mice. *Clin Cancer Res* **11**, 1551–1562.

[10] Luster TA, He J, Huang X, Maiti SN, Schroit AJ, de Groot PG, and Thorpe PE (2006). Plasma protein β-2-glycoprotein 1 mediates interaction between the anti-tumor monoclonal antibody 3G4 and anionic phospholipids on endothelial cells. *J Biol Chem* **281**, 29863–29871.

[11] Huang X, Bennett M, and Thorpe PE (2005). A monoclonal antibody that binds anionic phospholipids on tumor blood vessels enhances the antitumor effect of docetaxel on human breast tumors in mice. *Cancer Res* **65**, 4408–4416.

[12] He J, Yin Y, Luster TA, Watkins L, and Thorpe PE (2009). Antiphosphatidylserine antibody combined with irradiation damages tumor blood vessels and induces tumor immunity in a rat model of glioblastoma. *Clin Cancer Res* **15**, 6871–6880.

[13] He J, Luster TA, and Thorpe PE (2007). Radiation-enhanced vascular targeting of human lung cancers in mice with a monoclonal antibody that binds anionic phospholipids. *Clin Cancer Res* **13**, 5211–5218.

[14] Yin Y, Kavlie K, and Thorpe PE (2009). *Proceedings of the 100th Annual Meeting of the American Association for Cancer Research; Denver, CO*. American Association for Cancer Research, Philadelphia, PA. Abstract no. 5463.

[15] Digumarti R, Suresh AV, Bhattacharyya GS, Dasappa L, and Shan J (2010). Phase II study of bavituximab plus paclitaxel and carboplatin in untreated locally advanced or metastatic non–small cell lung cancer: interim results. *J Clin Oncol* **28**(15s), Suppl. Abstract 7589.

[16] Tabagari D, Nemsadze G, Janjalia M, Jincharadze M, and Shan J (2009). Phase II study of bavituximab plus docetaxel in locally advanced or metastatic breast cancer. *J Clin Oncol* **27**(15s), Suppl. Abstract 3005.

[17] Hsu AR, Cai W, Veeravagu A, Mohamedali KA, Chen K, Kim S, Vogel H, Hou LC, Tse V, Rosenblum MG, et al. (2007). Multimodality molecular imaging of glioblastoma growth inhibition with vasculature-targeting fusion toxin VEGF121/rGel. *J Nucl Med* **48**, 445–454.

[18] Zhou H, Luby-Phelps K, Mickey BE, Habib AA, Mason RP, and Zhao D (2009). Dynamic near-infrared optical imaging of 2-deoxyglucose uptake by intracranial glioma of athymic mice. *PLoS One* **4**, e8051.

[19] McCann CM, Waterman P, Figueiredo JL, Aikawa E, Weissleder R, and Chen JW (2009). Combined magnetic resonance and fluorescence imaging of the living mouse brain reveals glioma response to chemotherapy. *Neuroimage* **45**, 360–369.

[20] Rehemtulla A, Stegman LD, Cardozo SJ, Gupta S, Hall DE, Contag CH, and Ross BD (2000). Rapid and quantitative assessment of cancer treatment response using *in vivo* bioluminescence imaging. *Neoplasia* **2**, 491–495.

[21] Ke S, Wen X, Wu QP, Wallace S, Charnsangavej C, Stachowiak AM, Stephens CL, Abbruzzese JL, Podoloff DA, and Li C (2004). Imaging taxane-induced tumor apoptosis using PEGylated, ^{111}In-labeled annexin V. *J Nucl Med* **45**, 108–115.

[22] Schellenberger EA, Bogdanov A Jr, Petrovsky A, Ntziachristos V, Weissleder R, and Josephson L (2003). Optical imaging of apoptosis as a biomarker of tumor response to chemotherapy. *Neoplasia* **5**, 187–192.

[23] Kim YE, Chen J, Chan JR, and Langen R (2010). Engineering a polarity-sensitive biosensor for time-lapse imaging of apoptotic processes and degeneration. *Nat Methods* **7**, 67–73.

[24] Belhocine T, Steinmetz N, Hustinx R, Bartsch P, Jerusalem G, Seidel L, Rigo P, and Green A (2002). Increased uptake of the apoptosis-imaging agent ^{99m}Tc recombinant human annexin V in human tumors after one course of chemotherapy as a predictor of tumor response and patient prognosis. *Clin Cancer Res* **8**, 2766–2774.

[25] Kartachova MS, Valdes Olmos RA, Haas RL, Hoebers FJ, van Herk M, and Verheij M (2008). ^{99m}Tc-HYNIC-rh–annexin-V scintigraphy: visual and quantitative evaluation of early treatment-induced apoptosis to predict treatment outcome. *Nucl Med Commun* **29**, 39–44.

[26] Rottey S, Slegers G, Van Belle S, Goethals I, and Van de Wiele C (2006). Sequential ^{99m}Tc-hydrazinonicotinamide–annexin V imaging for predicting response to chemotherapy. *J Nucl Med* **47**, 1813–1818.

[27] Hammill AK, Uhr JW, and Scheuermann RH (1999). Annexin V staining due to loss of membrane asymmetry can be reversible and precede commitment to apoptotic death. *Exp Cell Res* **251**, 16–21.

[28] Andree HA, Reutelingsperger CP, Hauptmann R, Hemker HC, Hermens WT, and Willems GM (1990). Binding of vascular anticoagulant α (VACα) to planar phospholipid bilayers. *J Biol Chem* **265**, 4923–4928.

[29] Schlaepfer DD, Mehlman T, Burgess WH, and Haigler HT (1987). Structural and functional characterization of endonexin II, a calcium- and phospholipid-binding protein. *Proc Natl Acad Sci USA* **84**, 6078–6082.

[30] Jennewein M, Lewis MA, Zhao D, Tsyganov E, Slavine N, He J, Watkins L, Kodibagkar VD, O'Kelly S, Kulkarni P, et al. (2008). Vascular imaging of solid

tumors in rats with a radioactive arsenic-labeled antibody that binds exposed phosphatidylserine. *Clin Cancer Res* **14**, 1377–1385.

[31] Stafford JH and Thorpe PE (2011). Increased exposure of phosphatidylethanolamine on the surface of tumor vascular endothelium. *Neoplasia* **13**, 299–308.

[32] Giepmans BN, Adams SR, Ellisman MH, and Tsien RY (2006). The fluorescent toolbox for assessing protein location and function. *Science* **312**, 217–224.

[33] Hoffman RM (2005). The multiple uses of fluorescent proteins to visualize cancer *in vivo*. *Nat Rev Cancer* **5**, 796–806.

[34] Adams KE, Ke S, Kwon S, Liang F, Fan Z, Lu Y, Hirschi K, Mawad ME, Barry MA, and Sevick-Muraca EM (2007). Comparison of visible and near-infrared wavelength-excitable fluorescent dyes for molecular imaging of cancer. *J Biomed Opt* **12**, 024017.

[35] Hama Y, Urano Y, Koyama Y, Choyke PL, and Kobayashi H (2007). Activatable fluorescent molecular imaging of peritoneal metastases following pretargeting with a biotinylated monoclonal antibody. *Cancer Res* **67**, 3809–3817.

[36] Stummer W, Pichlmeier U, Meinel T, Wiestler OD, Zanella F, and Reulen HJ (2006). Fluorescence-guided surgery with 5-aminolevulinic acid for resection of malignant glioma: a randomised controlled multicentre phase III trial. *Lancet Oncol* **7**, 392–401.

[37] Sevick-Muraca EM, Sharma R, Rasmussen JC, Marshall MV, Wendt JA, Pham HQ, Bonefas E, Houston JP, Sampath L, Adams KE, et al. (2008). Imaging of lymph flow in breast cancer patients after microdose administration of a near-infrared fluorophore: feasibility study. *Radiology* **246**, 734–741.